optica

Injection locking of an electro-optomechanical device: supplementary material

CHRISTIAAN BEKKER, RACHPON KALRA, CHRISTOPHER BAKER*, AND WARWICK BOWEN

School of Mathematics and Physics, The University of Queensland, Australia

*Corresponding author: c.baker3@uq.edu.au

Published 29 September 2017

This document provides supplementary information to "Injection locking of an electro-optomechanical device," https://doi.org/10.1364/OPTICA.4.001196. It contains a detailed investigation into the effects of the inertial drive on op-tomechanical gain competition (section 1). We also provide additional details on the phase off-set between the mechanical oscillations and injection signal (2), the observed instability at large drive amplitudes (3) and the experimental setup (4 & 5).

https://doi.org/10.6084/m9.figshare.5370979

1. OPTOMECHANICAL MODE COMPETITION

Here we employ the numerical model described in the main text to investigate mechanical mode competition in an optomechanical resonator. Indeed, much like for the optical modes of a laser, different mechanical modes may compete for gain in an optomechanical resonator [1]. We show here how the electrical drive technique introduced introduced in this work and [2] may be used to permanently reorient the resonator's phase-space trajectory in order to, for instance, favor optomechanical gain for one mechanical mode versus another.

In order to illustrate this phenomenon, we consider for our simulation an optomechanical resonator with two distinct mechanical modes, chosen here to be at 6 MHz (mode 1) and 10 MHz (mode 2). We rewrite Eqs. 4 & 5 of the main text, to account for the presence of the second mechanical mode:

$$\dot{\alpha} = -\frac{\kappa}{2}\alpha + i(\Delta + G_1 x_1 + G_2 x_2)\,\alpha + A_L \qquad \textbf{(S1)}$$

$$m_{\mathrm{eff},1}\left[\ddot{x_1} + \Gamma_1 \dot{x_1} + \omega_{m,1}^2 x_1\right] = \hbar G_1 |\alpha|^2 + F_{\mathrm{d}}(t) \qquad \textbf{(S2)}$$

$$m_{\mathrm{eff},2}\left[\ddot{x_2} + \Gamma_2 \dot{x_2} + \omega_{m,2}^2 x_2\right] = \hbar G_2 |\alpha|^2 + F_{\mathrm{d}}(t), \qquad \textbf{(S3)}$$

where the subscripts 1 and 2 respectively refer to mechanical modes 1 and 2. Both mechanical modes may have a distinct effective mass m_{eff}, damping rate Γ, mechanical frequency ω_m and optomechanical coupling rate G, but both couple to the same intracavity field α.

Figure S1 demonstrates the effect of the external capacitive drive $F(d)$ on the optomechanical gain of each mechanical mode. The intracavity photon number $|\alpha|^2$ and cavity detuning Δ in the simulation are set such that each mechanical mode, taken individually, is above its regenerative oscillation threshold [3]. However, in the absence of drive ($V_{\mathrm{AC}} = F_d = 0$), mode 1 'wins' the gain competition and is the only mode to reach regenerative oscillation, i.e. 'phonon-lasing' (Fig. S1, top panel). This is visible by the large peaks at $\omega_{m,1}/2\pi$; $2\omega_{m,1}/2\pi$ and $3\omega_{m,1}/2\pi$ corresponding respectively to the fundamental mechanical frequency and first two higher order harmonics which appear due to the nonlinearity of the lorentzian optical resonance for large displacements [3]. Note also the absence of any peak at $\omega_{m,2}/2\pi$. Next, the drive force $F_d(t)$ is set to the frequency of mode 2 (10 MHz), and its amplitude is progressively increased ($V_{\mathrm{AC}} = 0.04; 0.05; 0.1$ V). The simulation results are plotted Fig. S1, second, third and fourth panels. For the highest drive voltage, the initial situation is completely reversed, with the noise peak corresponding to mode 2 now more than 30 dB above mode 1.

The transition between the two extreme cases is more quantitatively presented in Fig. S2(a), which presents the displacement amplitude of each mechanical mode in the steady-state, as a function of drive voltage. The transition from mode 1 to mode 2 having the largest displacement amplitude occurs abruptly, for $0.0425 < V_{\mathrm{AC}} < 0.045$ V. Similarly, Fig. S2(b) plots the phase-space trajectories of mode 1 (blue) and mode 2 (orange), for no capacitive drive ($V_{\mathrm{AC}} = 0$ V, top) and $V_{\mathrm{AC}} = 0.1$ V (bottom).

At this stage, we seek to verify that the switch from 'phonon-lasing' on mode 1 to mode 2 is indeed due to a change in the optomechanical gain experienced by both modes, and not to spurious effects due to the drive itself. In order to do so, we calculate the work done by the radiation pressure force on each mode during a mechanical oscillation. The radiation pressure force acting on mechanical mode i is given by $F_{\mathrm{rad},i} = \hbar G_i |\alpha|^2$, [3] such that the work performed by the intra-cavity optical field on mode i during one period is given by:

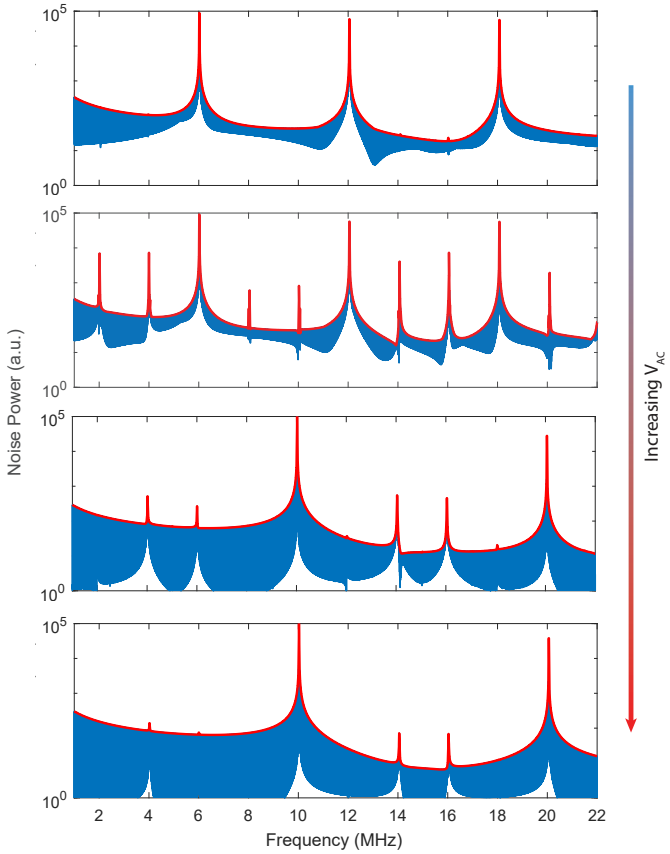

Fig. S1. Noise power spectra obtained through the FFT of the simulated normalized cavity output intensity (blue line). Red line (moving maximum) serves as a guide to the eye. Simulation parameters are as follows: $Q_{\text{opt}} = 2 \times 10^6$ (loaded); $\omega_{m,1}/2\pi = 6$ MHz; $\omega_{m,2}/2\pi = 10$ MHz; $\Gamma_1/2\pi = 6$ kHz; $\Gamma_2/2\pi = 10$ kHz (mechanical Q of both modes $= 1 \times 10^3$); $G_1/2\pi = G_2/2\pi = 1.9 \times 10^{18}$ Hz/m; $m_{\text{eff},1} = m_{\text{eff},2} = 5 \times 10^{-11}$ kg; laser power = 5 mW; $\Delta/2\pi = 35$ MHz; $dC/dx = 2 \times 10^{-9}$ N/V^2; $V_{\text{DC}} = 100$ V. From top to bottom panels, $V_{\text{AC}} = 0; 0.04; 0.05; 0.1$ V. Total simulation time 600 μs. In this simple model, we consider the effect of the drive F(d) to be identical on both mechanical modes, see Eqs. (S2) & (S3). Peaks appearing at e.g. 4 and 16 MHz correspond to sum- and difference frequency terms between modes 1 and 2. Simulation code available from the authors upon request.

$$W_{\text{rad},i} = \int_0^{T_i} \hbar G_i \, |\alpha|^2 \times \dot{x}_i \qquad \textbf{(S4)}$$

This work is calculated from our time-domain simulation, once the system has reached the steady-state. Results for modes 1 and 2 are plotted in Fig. S2(c), as a function of V_{AC}. We observe that the shift from 'phonon-lasing' on mode 1 to mode 2 is indeed accompanied by a more than two orders of magnitude change in the radiation-pressure work received by both modes (decrease for mode 1; increase for mode 2). This confirms that the change in dominant mechanical resonance is indeed due to gain competition between the two modes. We further verify that the work $W_{\text{d},i}$ done by the drive force

$$W_{\text{d},i} = \int_0^{T_i} F\,(d) \times \dot{x}_i, \qquad \textbf{(S5)}$$

remains always at least one order of magnitude below the radiation pressure work $W_{\text{rad},i}$.

Finally, we investigate what happens when the electrical drive is turned off after switching from mode 1 to mode 2. Does the system decay back to oscillating mainly on mode 1, or does it exhibit sufficient hysteresis to keep oscillating on mode 2? By replacing the drive term $F_d(t)$ in Eqs. (S2) and (S3) by $F_d(t)\,H(t_{\text{stop}} - t)$, where H is the Heaviside function, we turn off the electrical drive at a time t_{stop} once the system has been switched from mode 1 to mode 2. Even with the drive turned off, the system maintains regenerative oscillation on mode 2, indicating that the capacitive drive has effectively reoriented the resonator along a new stable oscillation trajectory, favoring optomechanical gain for a different mechanical mode.

The addition of an external driving means to a cavity optomechanical system may therefore enable dynamically adjusting the mechanical lasing mode, serve as a form of 'non-volatile' mechanical memory [4] (provided the optical input is not removed), and enable the exploration of normally inaccessible stable dynamical attractors of the system [5, 6].

2. PHASE OFFSET OF LOCKING AND EDGE-OF-LOCK EFFECTS

When a mechanical resonator is injection-locked, the phase of its motion maintains a constant offset with respect to the phase of the injection signal. The value of this phase offset depends on the detuning of the injection signal from the natural mechanical resonance frequency, as mentioned in the main text. We performed numerical simulations to investigate this dependence in each of the *quasi-lock* and *continuous* edge-of-lock regimes.

Our simulations consisted in solving the coupled differential equations that govern the time evolution of the optical and mechanical degrees of freedom (Eqs. 4 & 5 of the main text). These were solved using an ODE solver (MATLAB) to determine the dynamics of the optomechanical system over a time period on the order of ~1000 μs, with a few million time steps –corresponding to an average nanosecond-range time increment between successive points. Note that these simulations, even though simplified (they do not include thermo-optic effects or a random thermal force for instance), are nevertheless able to accurately reproduce our experimental observations (see Fig. 5 of the main text). This holds for both the quasi-lock and continuous regimes. The simulation code is available from the authors upon request.

Our numerical modelling reveals that the dependency of the phase offset on the frequency of the injection tone is qualitatively different between the two regimes, as shown in Fig. S3. Figure S3(a) plots the phase offset between electrical drive and locked mechanical oscillator, as function of drive frequency, for simulation parameters corresponding to the quasi-lock regime. The locking here spans approximately from 8.920 MHz to 8.938 MHz, corresponding to a locking range of 18 kHz. The phase offset is in very good agreement to that expected from the theory of an injection-locked tank circuit [7]. The phase offset spans the expected $[-\pi/2; \pi/2]$ range, with zero phase offset in the center of the lock range, and an offset approaching $\pm\pi/2$ at the edges of the lock range [7].

In striking contrast to the quasilock case, in the continuous regime the phase offset is bound within $[-\pi; 0]$, with a non-symmetric relationship of the phase-offset with respect to the center of the locking range. Another unique feature of this regime is the apparently 'instantaneous' jump of the phase offset

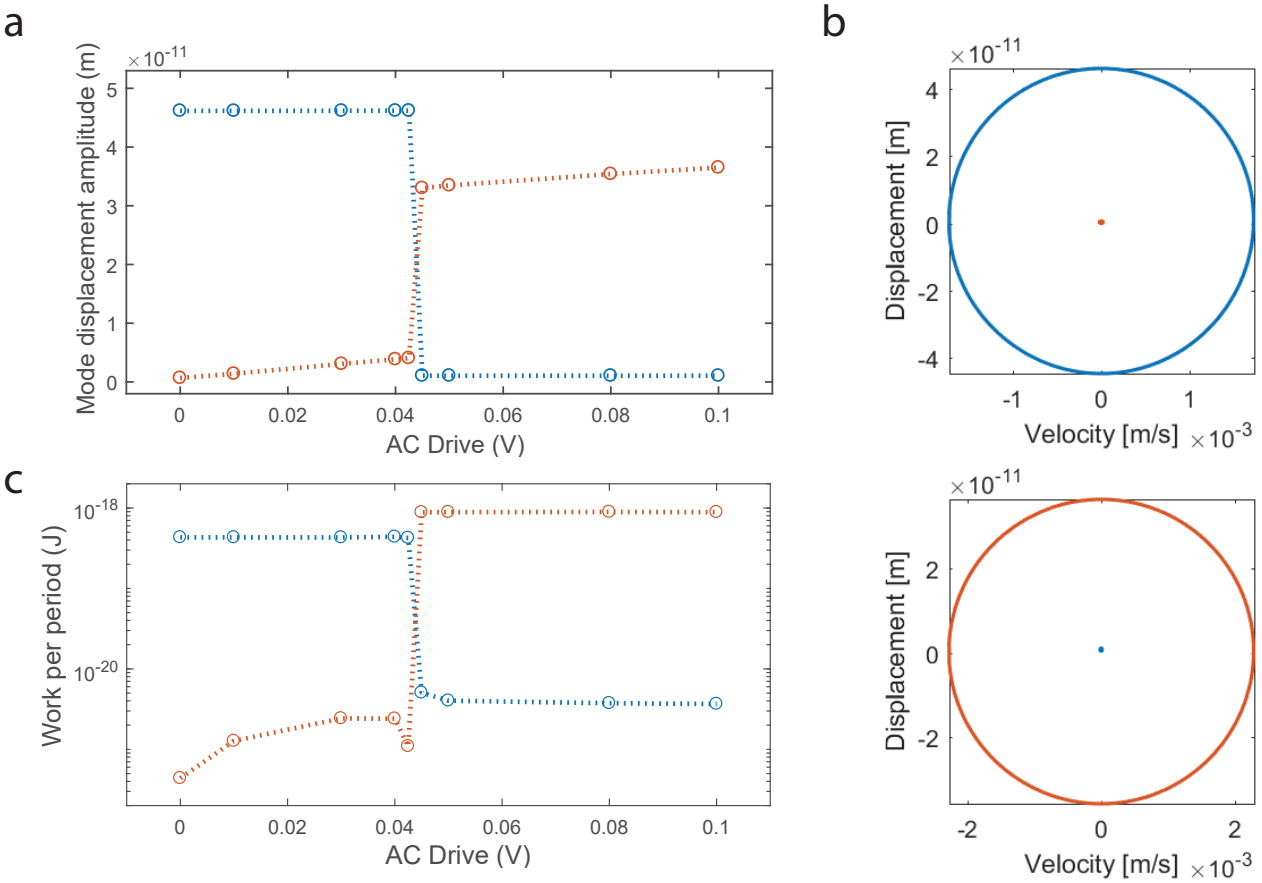

Fig. S2. (a) Simulated steady-state mechanical displacement amplitude of mode 1 (blue) and mode 2 (orange), as a function of AC drive voltage. (b) Phase-space trajectories of mode 1 (blue) and mode 2 (orange), for no capacitive drive ($V_{\mathrm{AC}} = 0$ V, top) and $V_{\mathrm{AC}} = 0.1$ V (bottom). (c) Work W_{rad} performed by the intra-cavity optical field on mode 1 (blue) and mode 2 (orange) during one oscillation period. This corresponds to a net power transferred from the light field to the lasing mechanical mode on the order of a few picoWatts.

from $-\pi$ to $-\pi/2$ close to the lower end of the locking range (8.913 MHz). Near the edge of the locking range, the phase offset oscillates in time around a steady-state value, as shown in Fig. S4(b). This oscillation is responsible for the increased uncertainty in defining the value of the phase offset, as evidenced by the growing error bars.

We now look at the behaviour of the phase offset in the time domain, for a drive frequency just on the edge of the lock range. This analysis reveals a qualitatively different mechanism through which the locking is lost in both quasi-lock and continuous regimes. Figure S4 plots the phase offset between the mechanical oscillator position x and the injection signal as a function of time. In Fig. S4(a) the phase offset is shown for a drive frequency just outside the lock range, corresponding to a drive at 8.940 MHz in Fig. S3(a). Since this drive is outside of the locking range, the phase offset is no longer constant over time. Nevertheless, the phase offset is maintained at $\pi/2$ modulo 2π for sustained periods of time (horizontal sections of the curve), before incurring a 2π phase slip, and locking again. The mechanical oscillator therefore alternates between periods of time where it is locked to the drive, and periods where it is not. This regime is therefore named the *quasi-lock* or *phase-slip* regime [7]. As the drive frequency is further moved away from the edge of the locking range, the fraction of the time the oscillator is locked versus slipping keeps diminishing. This is the mechanism whereby lock is lost in the quasilock regime.

In contrast, Fig. S4(b) plots the phase offset in the continuous regime for a drive frequency just on the edge of the lock range (corresponding to the rightmost point in Fig. S3(b)). The simulation shows an initially unlocked oscillator which locks after four 2π phase slips. After locking, no further phase-slips occur. Nevertheless, the phase offset oscillates about the value of 8π (corresponding to 0 mod 2π in Fig. S3(b)). The further the drive frequency is moved away from the center of the lock range, the larger these phase oscillations become (as illustrated Fig. S3(b)), until lock is lost. This analysis therefore underlines the qualitative differences between the quasi-lock and continuous regimes, both in terms of the phase offset inside the locking range, as well as the mechanism whereby the oscillator falls out of lock. Further research must be done to investigate other differences between these regimes, and uncover the precise mechanisms behind such qualitatively different behaviour.

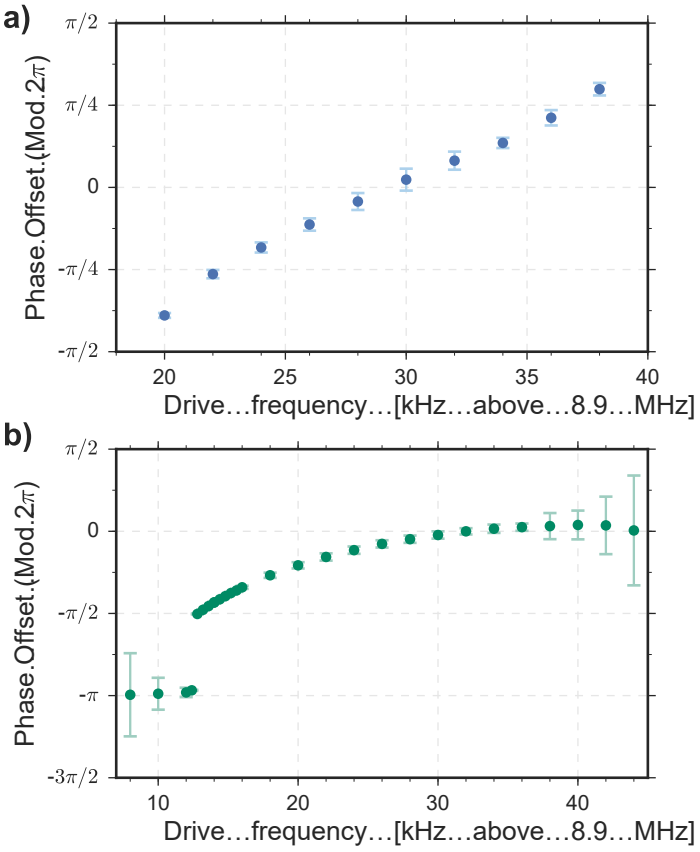

Fig. S3. Phase offset between the injection signal and the locked oscillations as a function of the drive frequency. The phase offset is measured between the electrical drive and the resonator position x, once the system has reached its steady-state in the simulation. These were numerically modelled in the **a)** quasilock and **b)** continuous regimes. Note how the behaviour of the phase offset is qualitatively different between the two regimes.

3. INSTABILITY OF LARGE DRIVES

As shown in the main text, we attempt to tune the regenerative oscillation frequency across a 71 kHz locking range using a $V_{AC} = 5$ V drive. However, we find that when the frequency of this strong drive is set close to the mechanical resonance frequency, the optical cavity is shifted out of resonance and regenerative oscillations cease. On the other hand, when the frequency of the drive is set away from resonance, regenerative oscillations remain stable and successfully lock to the drive tone. We suspect that this occurs due to a combination of large amplitude mechanical oscillations when driven near resonance along with thermal effects in the silica microtoroid [8]. Silica has an appreciable thermo-optic coefficient, which describes the change in its refractive index with temperature. In effect, the optical resonance frequency shifts as the optical power inside the cavity is increased, resulting in optical bi-stability [9]. These shifts are routinely observed in the experiment through frequency scans of the optical mode, which produce a characteristic triangular shape [10]. When driven near resonance to high amplitudes, the mechanical oscillations can sufficiently shift the optical resonance away from the laser frequency ($Gx > \kappa$) such that the optical power inside the cavity drops significantly. This results in a run-away effect where the silica cools as the resonance frequency continues to shift further away from the laser frequency until it reaches its equilibrium temperature, where the laser frequency is completely detuned from resonance.

4. ELECTRIC PROBE SETUP

Electrical contact with our device is established through firmly pressing ultrasharp tungsten probes with tip radii of 1 μm onto the contact pads at the center of the resonator. We observe that, over time, the probes cause wear to the pads with each application, particularly when a DC voltage is applied across the electrodes. Tungsten is a very porous material, and oxide tends to build up on and within the probe. This accumulation of oxide can create a high contact resistance between the probe and the pad, with the potential for an applied voltage to cause arcing [11], which we suspect is the cause of the observed wear. This problem may be avoided by using beryllium copper (BeCu) probe tips. These are softer than tungsten tips and are effectively polished when pressed against a surface. As the BeCu

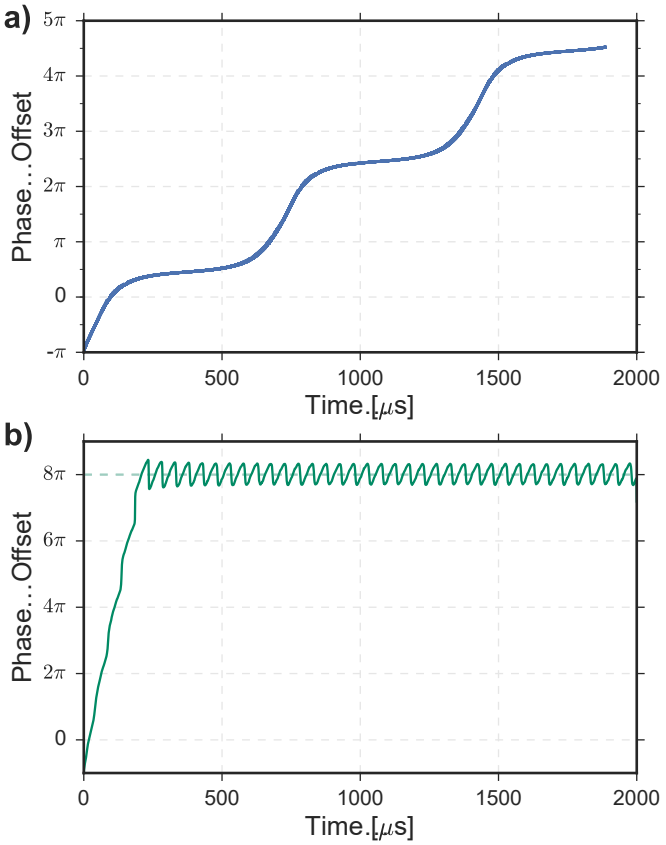

Fig. S4. Phase offset as a function of time between the mechanical oscillator position x and the injection signal. a) Simulated phase offset in the quasilock regime for a drive frequency just outside the lock range (8.940 MHz). The quasi-locking regime corresponds to the 'phase-slip' regime described by Razavi [7], where the oscillator is being held at a phase offset of $\pi/2$ modulo 2π for periods of time, before incurring a 2π phase slip. b) Phase offset in the continuous regime for a drive frequency just on the edge of the lock range (8.944 MHz - rightmost point in Fig. S3(b)) . The green dotted line corresponds to a phase offset of 0 modulo 2π, shown in Fig. S3(b).

probe tip slides, the scrubbing action leaves the tip surface clean, maintaining its low contact resistance with the gold pads [11].

5. FIBRE TAPER STABILISATION

All measurements shown in the main text are performed with the tapered section of the fibre brought into contact with the top of the silica microtoroid. This is done out of necessity, as we are unable to achieve stable coupling of the optical cavity to the fibre while simultaneously applying a DC voltage to the electrodes and keeping the fibre positioned in proximity to the device. Invariably, the fibre drifts and is pulled towards the device in timescales on the order of one minute, likely due to polarization of the fibre and a resulting attractive force. With the voltage switched off, however, we are able to take measurements to extract the mechanical linewidth without the fibre touching. This comparison reveals that bringing the fibre into contact with the device only reduces the mechanical quality factor by a factor of ~ 3. Fortunately, the presence of the fibre on top of the microtoroid does not severely damp the radial motion of the mechanical resonator. With the fibre in contact, stable regenerative oscillations are maintained for hours.

For future devices, there are a number of ways in which stable optical coupling can be achieved without bringing the fibre into contact with the microtoroid. For instance, separate support structures such as nanoforks or support pads can be fabricated to stabilize the fibre [10, 12]. Alternatively, the tapered fibre can be removed completely and integrated waveguides for optical coupling can be used instead [13, 14].

REFERENCES

1. U. Kemiktarak, M. Durand, M. Metcalfe, and J. Lawall, "Mode Competition and Anomalous Cooling in a Multimode Phonon Laser," Physical Review Letters **113** (2014).
2. C. G. Baker, C. Bekker, D. L. McAuslan, E. Sheridan, and W. P. Bowen, "High bandwidth on-chip capacitive tuning of microtoroid resonators," Optics Express **24**, 20400 (2016).
3. M. Aspelmeyer, T. J. Kippenberg, and F. Marquardt, "Cavity optomechanics," Reviews of Modern Physics **86**, 1391–1452 (2014).
4. M. Bagheri, M. Poot, M. Li, W. P. H. Pernice, and H. X. Tang, "Dynamic manipulation of nanomechanical resonators in the high-amplitude regime and non-volatile mechanical memory operation," Nature Nanotechnology **6**, 726–732 (2011).
5. F. Marquardt, J. G. E. Harris, and S. M. Girvin, "Dynamical Multistability Induced by Radiation Pressure in High-Finesse Micromechanical Optical Cavities," Physical Review Letters **96** (2006).
6. A. G. Krause, J. T. Hill, M. Ludwig, A. H. Safavi-Naeini, J. Chan, F. Marquardt, and O. Painter, "Nonlinear Radiation Pressure Dynamics in an Optomechanical Crystal," Physical Review Letters **115** (2015).
7. B. Razavi, "A study of injection locking and pulling in oscillators," IEEE Journal of Solid-State Circuits **39**, 1415–1424 (2004).
8. T. McRae, K. H. Lee, M. McGovern, D. Gwyther, and W. Bowen, "Thermo-optic locking of a semiconductor laser to a microcavity resonance," Optics express **17**, 21977–21985 (2009).
9. V. R. Almeida and M. Lipson, "Optical bistability on a silicon chip," Optics letters **29**, 2387–2389 (2004).
10. J. Rosenberg, Q. Lin, and O. Painter, "Static and dynamic wavelength routing via the gradient optical force," Nature Photonics **3**, 24 (2009).
11. Several technical documents about the use of probes and wire bonding for industrial electronics applications deals with this. A particular document dealing with probe materials was published by Accuprobe, inc. as a technical bulletin, viz. Probe Tips 10: Tip Material, Shape and Size. See https://www.bita.se/bitase1/datasheets/AccuPT2010TipMaterialSizeandShape[1]-SE-LU.pdf.
12. D. McAuslan, G. Harris, C. Baker, Y. Sachkou, X. He, E. Sheridan, and W. Bowen, "Microphotonic Forces from Superfluid Flow," Physical Review X **6**, 021012 (2016).
13. S. Tallur, S. Sridaran, and S. a. Bhave, "A monolithic radiation-pressure driven, low phase noise silicon nitride opto-mechanical oscillator," Optics Express **19**, 24522–24529 (2011).
14. C. Baker, C. Belacel, A. Andronico, P. Senellart, A. Lemaitre, E. Galopin, S. Ducci, G. Leo, and I. Favero, "Critical optical coupling between a GaAs disk and a nanowaveguide

suspended on the chip," Applied Physics Letters **99**, 151117 (2011).